AXONAL BOUTON MODELING, DETECTION AND DISTRIBUTION ANALYSIS FOR THE STUDY OF NEURAL CIRCUIT ORGANIZATION AND PLASTICITY

Christina A. Hallock [2]*, Inci Özgüneş*[1]*, Ramamurthy Bhagavatula*[2]*, Gustavo K. Rohde*[1]*,*
Justin C. Crowley[3]*, Christina E. Onorato*[3]*, Abhay Mavalankar*[2]*, Amina Chebira*[1]*,*
Chuen Hwa Tan[1]*, Markus Püschel*[2] *and Jelena Kovačević*[1,2]

[1] Dept. of Biomedical Engineering and Center for Bioimage Informatics
[2] Dept. of Electrical and Computer Engineering
[3] Dept. of Biological Sciences and Center for the Neural Basis of Cognition
Carnegie Mellon University, Pittsburgh, PA, USA

ABSTRACT

We propose a novel method for axonal bouton modeling and automated detection in populations of labeled neurons, as well as bouton distribution analysis for the study of neural circuit organization and plasticity. Since axonal boutons are the presynaptic specializations of neural synapses, their locations can be used to determine the organization of neural circuitry, and in time-lapse studies, neural circuit dynamics. We propose simple geometric models for axonal boutons that account for variations in size, position, rotation and curvature of the axon in the vicinity of the bouton. We then use the normalized cross-correlation between the model and image data as a test statistic for bouton detection and position estimation. Thus, the problem is cast as a statistical detection problem where we can tune the algorithm parameters to maximize the probability of detection for a given probability of false alarm. For example, we can detect 81% of boutons with 9% false alarm from noisy, out of focus, images. We also present a novel method to characterize the orientation and elongation of a distribution of labeled boutons and we demonstrate its performance by applying it to a labeled data set.

Index Terms— axonal bouton modeling, bouton distribution analysis, neural circuit organization and plasticity, light microscopy, confocal microscopy, two-photon microscopy, neuron, neuroanatomy

1. INTRODUCTION

An important part of modern neuroscience research aims to elucidate the mechanisms underlying brain development and neural plasticity, by collecting image data spanning several resolutions and modalities, and extracting relevant functional and structural information. One vital component for the understanding the developmental dynamics of the visual cortex is a bouton. Boutons are swellings on axons that contain the cellular machinery for neurotransmitter release, including neurotransmitter filled vesicles. Identification of boutons at the resolution of the light microscope has been shown to be reliable and indicative of one or more synapses through confirmation by electron microscopy [1, 2]. Thus, in single time point experiments, boutons indicate where a neuron sends its information. In time-lapse, live tissue work, one can use bouton stability and change as a measure of synaptic change in the brain [3, 4].

In general, bouton locations and distribution of their locations are both used as experimental evidence (dependent variables) in a variety of studies in systems neuroscience. In the field of visual neuroscience, problems of interest include the exploration of developmental dynamics before and during the critical period in the visual cortex. For example, bouton locations and distributions in the superficial layers of visual cortex provide the neuroscientist with a key to the circuitry of visual cortex associated with orientation selectivity [5, 6]. The Crowley Lab is interested in combining the efficiency of present day imaging devices, axonal tracing, and bouton distribution analysis techniques, to explore how stimulus features are represented in the activity of identified neural circuitry. Unfortunately, bouton detection is currently performed manually; given the vast amount of images that are collected in a very short time, and the fact that the human brain has about 10^{15} synapses, this leads to an inefficient and error-prone way to extract information out of the images.

Currently, as the automated bouton detection is not available, we set this as the first goal of our work. To achieve it, we develop simple models for a bouton along an axon that account for variations in size, position, rotation, and curvature of the axon in the vicinity of the bouton. We use these models as templates and compute the normalized cross-correlation [7] between an image and these templates, along with thresholding, to detect the bouton locations in the image. The detection performance can be traded off with the number of false alarms by choosing the detection threshold appropriately with the aid of a receiver operating characteristic (ROC) curve.

Once the relevant neurological information is extracted (bouton locations in this case), biologists need various quantitative measures to characterize the developmental dynamics of the visual cortex. As mentioned previously, the directionality of the bouton distribution has been shown to be indicative of various stages in the development of the visual cortex. While a possible measure is the orientation selectivity index (OSI) [8], it does not identify the actual direction nor does it detect a lack of symmetry in the distribution. We propose a new measure, the *anisotropy selectivity index (ASI)*, which is more sensitive than the OSI and addresses the above problems.

This work was supported in part by NSF through awards CCF-0515152 and EF-0331657, the PA State Tobacco Settlement, Kamlet-Smith Bioinformatics Grant, Searle Scholar Award, Dana Foundation Program in Brain and Immuno Imaging, Human Frontiers Science Program, A.P. Sloan Research Fellowship and Howard Hughes Medical Institute. Chuen Hwa Tan is now with Oracle; she performed the work while at Carnegie Mellon University.

2. BOUTON MODELING, DETECTION AND ESTIMATION

Bouton Modeling. A simple model for a bouton can be viewed as a pearl on a string: a circular structure (bouton) placed on an elongated tubular structure (axon), with possible curvature. In Fig. 1, top, we show a few examples of boutons extracted from a negative of a brightfield image with a magnification of 63x together with the corresponding geometric models (bottom). Among the models, we have a bouton on a straight axon and a bouton on a curved axon. One can also model a terminal bouton, not shown here. The bouton size and shape as well as the axon curvature and width can be varied. Finally, the model can also be rotated by an arbitrary angle.

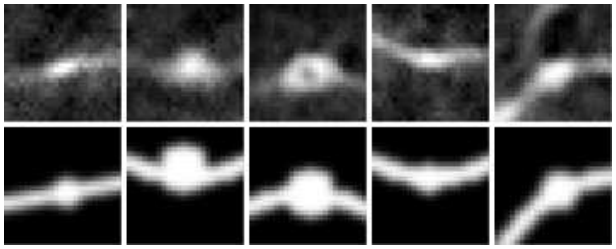

Fig. 1. Illustration of bouton models: In the top row, we show a few examples of boutons extracted from a negative of a brightfield image. These boutons can vary in size and rotation, and the axon may curve in the vicinity of the bouton. In the bottom row we show corresponding bouton models mimicking the actual boutons shown above them. Observe that we have a model of a bouton on a straight axon and a bouton on a curved axon, with various bouton sizes. The first model is at 10 degrees and the last model at 30 degrees, while the other models are either at 0 or 180 degrees.

Bouton Detection and Estimation. To estimate and detect boutons, we first incorporate a given model into a 2D template of size $m \times n$ pixels. The resolution of the image is used to translate actual measurements in μm of axon width and bouton radius into pixels. Then, to find the bouton locations in an image, we use the normalized cross-correlation γ, between the image f and the model t at (u, v) (see (1)). By using normalized cross-correlation as opposed to traditional cross-correlation, we ensure that our detections are tolerant to changes in image intensity [7].

$$\gamma = \frac{\sum[f(x,y) - \bar{f}_{u,v}][t(x-u, y-v) - \bar{t}]}{\sqrt{\sum[f(x,y) - \bar{f}_{u,v}]^2 \sum[t(x-u, y-v) - \bar{t}]^2}}, \quad (1)$$

The sums above are computed over (x, y) under the window containing the model t positioned at (u, v), $\bar{t}$ is the mean of the model and $\bar{f}_{u,v}$ is the mean of $f(x, y)$ in the region under the model. After the correlation, the resulting image will have values ranging from -1 to 1. We extract the locations whose correlation coefficients are greater than that of a global threshold parameter T; its value can be set to accommodate a trade-off between the probability of correct detections and the probability of false alarms (an undesirable outcome from the biological point of view).

We repeat the process of normalized cross-correlation and thresholding for each of the various models described previously. For each model, since an axon and bouton can occur at any orientation in an image, we iterate through several rotations of the model. After applying the chosen threshold, the peak location corresponding to the largest value of the correlation coefficient is stored. We also impose a minimum radius $R_{\min}$ within which there can only be one peak; in other words, two boutons cannot be closer than $R_{\min}/2$. (This minimum radius is based on the bouton size and the axon width and it does play an important role in eliminating false alarms.) Once we exhaust our model space, we look through the peak locations accumulated over the search space, and choose those whose cross-correlation values are the highest, again enforcing a minimum radius within which there can only be one peak.

Data Set. Tissue preparation was similar to previously published protocols [6]. All procedures were approved by the Duke University institutional animal care and use committee. Histology specimens on glass slides were transferred to Carnegie Mellon University for further analyses.

Neural Tracer Injections. Iontophoretic injections were made with microdot glass micro pipettes with a tip diameter of $\sim 10\mu$m containing 5% biocytin (Sigma, St. Louis, MO) in saline using pulsed current (7 sec on, 7 sec off) of 2.5 mamps for 10-15 min. After the injection the animal was sutured and returned to its cage.

Tissue Processing. After a 16-hr recovery period, the animal was deeply anesthetized with Nembutal (25 mg, i.p.) and transcardially perfused with 0.9% saline, followed by 10% formalin in 0.1 M sodium phosphate buffer. The brain was removed and a block of cortex containing V1 was flattened while immersed in 20% sucrose in 0.1 M sodium phosphate buffer and maintained at 48C overnight. The following day, 40 mm tangential sections were cut from the block on a freezing microtome. Procedures for visualization of the biocytin label have been published previously [9]. Briefly, goat anti-biotin and biotinylated rabbit anti-goat antibodies (Vector Laboratories, Burlingame, CA) were used to amplify the signal before processing with the standard avidin-biotin complex (Vectastain Kit PK-4000, Vector, Burlingame, CA) reaction, and diaminobenzidine with nickel and cobalt intensification.

Imaging. 12-bit brightfield images (1344 $\times$ 1024) were acquired with a Hamamatsu ORCA ER-AG CCD camera coupled with a 0.63x reduction optic to a Zeiss Axioplan 2 microscope fitted with a Plan-Apochromat 63x (1.4 NA) oil immersion objective. The ground truth is obtained by having an expert mark the bouton locations.

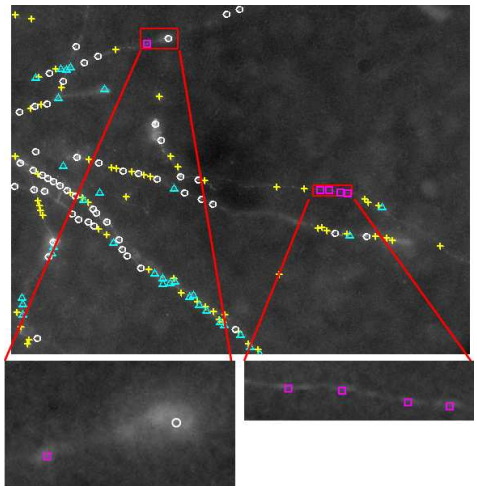

Fig. 2. Locations of correctly detected (circles), missed (triangles) and incorrectly detected boutons (+'s). We have also isolated false alarms that lie on what we believe to be boutons not labeled in the ground truth (squares).

Results. To illustrate the effect of a threshold, Fig. 2 shows an example with $T = 0.875$ and $R_{\min} = 10$ pixels (1.6 μm) where the locations of the correctly detected (circles), missed (triangles) and incorrectly detected (+'s) boutons are marked.

The performance of the bouton detection algorithm can be assessed, in a statistical sense, using an ROC curve, where, for a given set of parameters in the detection algorithm, the probability of mislabeled boutons is plotted against the probability of correct detections. In our case, these were computed empirically by comparing the results produced by our algorithm against ground truth data. The ROC curve also allows one to choose a threshold that satisfies some probability of false detections, or correct detections. In Fig. 3 (top), we set $R_{\min} = 10$ pixels and trace the ROC curve shown in the same figure (bottom). Each data point on the curve correspond to a different T. For example, the result shows that the method can detect 81% of the boutons with 9% false alarm rate. Interestingly enough, although the manually marked boutons are used as ground truth, these are not perfect, that is, experts miss boutons on occasion (we show examples of such misses in Fig. 2). Some of these have been marked by our algorithm as false alarms, although in reality, they are boutons missed during manual process.

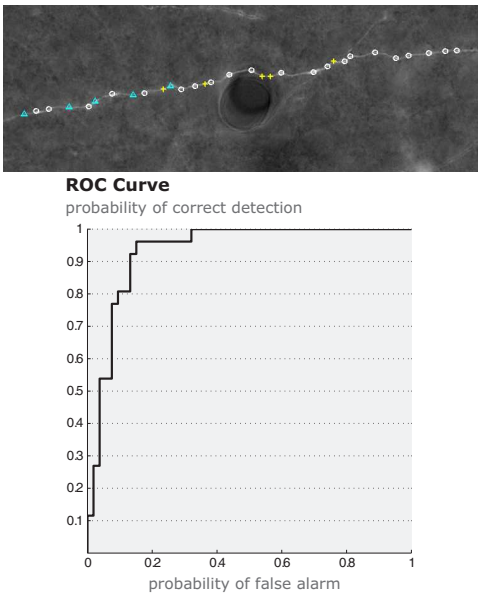

Fig. 3. An image with bouton detection results (top) and its corresponding ROC curve with $R_{\min} = 10$ pixels (1.6 μm, bottom).

Due to our method of sorting and pruning multiple detections that are in the vicinity of each other, we cannot generate a complete ROC curve by incrementing our detection threshold through all possible values; rather, our thresholds range from 0.75 to 1.00 in steps of 0.001. The true number of false alarms possible is that generated by using a threshold of -1 which we cannot simulate due to complexity. Ignoring our method of eliminating multiple proximal detections, the maximum number of false alarms in an image of size $m \times n$ pixels, given that there are N boutons in an image, would be $m \times (n - N)$. However, our algorithm reduces this to an unquantifiable number, and thus, our maximum number of false alarms is generated using a threshold of 0.75. In order to normalize the axes of our ROC curve to the traditional [0, 1] range, we choose to divide the number of true detections and the number of false alarms, by the number of labeled boutons in the ground truth and the maximum number of false alarms, respectively. We are in fact normalizing by a number that is significantly smaller than the "true" maximum number of false alarms, resulting in a probability of false alarm that is in fact higher than it should be.

3. BOUTON DIRECTIONALITY ANALYSIS

We now show one example of the type of analysis needed once the bouton locations have been extracted. This analysis will be performed on a different data set, one that has already been labeled.

Neuroscientists study bouton distribution as it gives useful information about a developmental stage and condition. In general, an animal's visual cortex cells are more directional as that animal reaches adulthood. Qualifying the distribution as "more directional" means simply that the labeled axons and boutons extend for longer distances, are more densely distributed and give off more terminal boutons, all this along an axis in the map of visual space that corresponds to the preferred orientation of the injection site.

Orientation Selectivity Index. Currently, there is no standard measure available to characterize directionality of bouton distribution. A possible measure is the OSI index proposed in [8], which uses Fourier analysis to quantify directionality as follows:

$$\text{OSI} = \frac{A_2}{A_0 + A_2}, \tag{2}$$

where A_0 is the DC component of the Fourier transform, while A_2 is the second harmonic. In the above, the input boutons are typically divided into 36 bins, each encompassing $10\,\text{deg}$ to create a histogram on which the Fourier transform is applied. The OSI value is typically expressed in $\%$, and the higher the percentage, the more directional the distribution. The meaning behind the second harmonic is that two peaks, equidistant on the unit circle, would appear, denoting a single direction.

The issues with the OSI are that the it does not identify the actual direction nor does it detect a lack of symmetry in the distribution of the boutons (actually, for the measure to be valid, the distribution must be symmetric).

Anisotropy Selectivity Index. Inspired by anisotropy measures for quantifying diffusion profiles [10], we propose a new measure called *anisotropy selectivity index (ASI)* to quantify the directionality of the bouton distribution. It is defined as

$$\text{ASI} = 2\left(\frac{\lambda_1}{\lambda_1 + \lambda_2} - 0.5\right), \quad \text{with } \lambda_1 \geq \lambda_2, \tag{3}$$

where $\lambda_{1,2}$ are the eigenvalues of the following matrix:

$$S = \frac{1}{N}\sum_{i=1}^{N} q_i q_i^T, \tag{4}$$

with q_i the vectors of bouton locations. Again, we express ASI in percentages; the higher the ASI, the more directional the distribution. Moreover, the eigenvalues as well as the corresponding eigenvectors give information about the major axis of bouton distribution.

Data Set. We used bouton distribution data from layers 2 and 3 of the primary visual cortex of tree shrews of various ages. We had 10 data sets; 3 at 14 days, 1 at 18 days, 1 at 21 days, 1 at 22 days, 1 at 29 days, 1 at 43 days and 2 adult ones. To ensure none of the boutons are missed, they have been marked by a human expert.

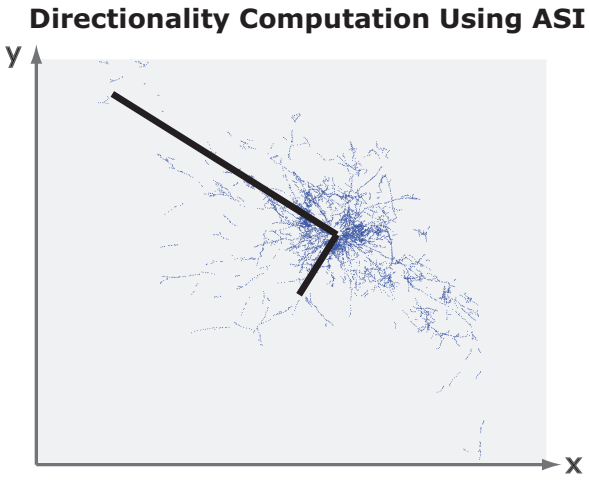

Fig. 4. Illustration of directionality computation on the spatial distribution of boutons using ASI. The two bold vectors are the eigenvectors of S with the larger one corresponding to eigenvalue λ_1. The plot clearly demonstrates the directionality of the bouton distribution.

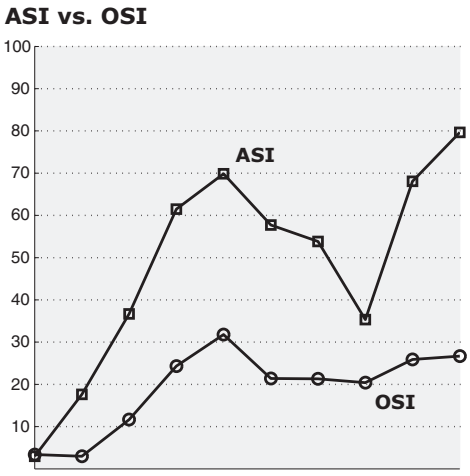

Fig. 5. ASI (squares) vs OSI (circles) plotted against the increasing developmental age. Both measures follow a similar trend with ASI displaying more sensitivity.

Results. Fig. 4 shows the bouton distribution on one data set with the ASI index 57.73% and the directionality vectors superimposed. The larger vector clearly shows the main direction of the bouton distribution, with a quantitative measure attached. Remember that while OSI would have detected presence of directionality, it would have not given any indication of the actual direction.

Fig. 5 demonstrates two important points. First, it plots both ASI and OSI for all 10 data sets. While it is clear that both measures follow similar trends, that is, they would give similar qualitative idea about the degree of directionality of the bouton distribution, the ASI measure is more sensitive. Moreover, as the measures are plotted against the developmental age, one can see how the directionality behaves as the age increases. As we did not have access to enough data sets, we will not be drawing any biological conclusions at this point; this is left for future work. We are currently investigating a few properties of the ASI measure, such as its ability to measure symmetry and give information about directionality as a function of distance from the injection site, as well as methods to quantify clustering of data.

4. CONCLUSIONS AND FUTURE WORK

We have begun our quest towards the automated extraction and quantification of neurological information from image data with an automated algorithm for bouton detection as well as a new measure of bouton distribution directionality and elongation. Our algorithm extracts boutons with high fidelity; reducing and/or eliminating false positives is the task for future work. On the analysis side, we are investigating both how to extend the ASI measure as well as new measures of quantifying bouton distribution directionality (such as nonrandom clustering).

Acknowledgments. We are grateful to Dr. David Fitzpatrick, Department of Neurobiology, Duke University Medical Center, for providing access to the shrew samples.

5. REFERENCES

[1] S. M. Lu and R. C. Lin, "Thalamic afferents of the rat barrel cortex: a light- and electron-microscopic study using phaseolus vulgaris leucoagglutinin as an anterograde tracer," *Somatosens Mot Res*, vol. 10, pp. 1–16, 1993.

[2] J. C. Anderson, T. Binzegger, K. A. Martin, and K.S. Rockland, "The connection from cortical area V1 to V5: A light and electron microscopic study," *Journ. Neuroscience*, vol. 18, pp. 10525–10540, 1998.

[3] V. De Paola, A. Holtmaat, G. Knott, S. Song, L. Wilbrecht, P. Caroni, and K. Svoboda, "Cell type-specific structural plasticity of axonal branches and boutons in the adult neocortex," *Neuron*, vol. 49, pp. 861–875, 2006.

[4] D. D. Stettler, H. Yamahachi, W. Li, W. Denk, and C. D. Gilbert, "Axons and synaptic boutons are highly dynamic in adult visual cortex," *Neuron*, vol. 49, pp. 877–887, 2006.

[5] C. D. Gilbert and T. N. Wiesel, "Columnar specifity of intrinsic horizontal and corticocortical connections in cat visual cortex," *Journ. Neuroscience*, vol. 9, pp. 2432–2442, 1989.

[6] W. H. Bosking, Y. Zhang, B. Schofield, and D. Fitzpatrick, "Orientation selectivity and the arrangement of horizontal connections in tree shrew striate cortex," *Journ. Neuroscience*, vol. 17, no. 6, pp. 2112–2127, Mar. 1997.

[7] J. P. Lewis, "Fast normalized cross-correlation," http://www.idiom.com/∼zilla/Papers/nvisionInterface/.

[8] B. Chapman and M. P. Stryker, "Development of orientation selectivity in ferret visual cortex and effects of deprivation," *Journ. Neuroscience*, vol. 13, no. 12, pp. 5251–5262, Dec. 1993.

[9] W. M. Usrey and D. Fitzpatrick, "Specificity in the axonal connections of layer VI neurons in tree shrew striate cortex: Evidence for distinct granular and supragranular systems," *Journ. Neuroscience*, vol. 16, pp. 1203–1218, 1996.

[10] C. Pierpaoli and P. J. Basser, "Toward a quantitative assessment of diffusion anisotropy," *Magn. Reson. Med.*, vol. 36, pp. 893–906, 1996.